Airfoil drag elimination and stall suppression via piezoelectric dynamic tangential synthetic jet actuators

Ron Barrett[*a,b], Jeremy Corpening[*b,c] and Christopher Reasonover[*b,d]
[a]Faculty of Aerospace Engineering, Technical University of Delft, Netherlands
[b]Aerospace Engineering Department, Auburn University, Alabama
[c]Aerospace Engineering Department, Purdue University, West Lafayette, Indiana
[d]Naval Surface Warfare Center, Dahlgren, Virginia

ABSTRACT

This paper describes a new method for drag elimination and stall suppression via tangential synthetic jet actuators. This boundary layer control (BLC) method is shown to perform as well as continuous and normal synthetic jet BLC methods but without fouling difficulties, system-level complexity or extreme sensitivity to Reynolds number. Classical laminated plate theory (CLPT) models of the piezoelectric actuators were used to estimate diaphragm deflections and volume per stroke. A 12" (30.5cm) chord, 6" (15.3cm) span NACA 0012 profile wing section was designed with three unimorph 10 mil (254µm) thick, 3.25" (8.23cm) square piezoelectric diaphragm plenums and five 1 mil (25µm) thick stainless steel valves spaced from 15%c to the trailing edge of the airfoil. Static bench testing showed good correlation between CLPT and experiment. Plenum volume per stroke ranged up to 5cc at 500 V/mm field strength. Dynamic testing showed resonance peaks near 270 Hz, leading to flux rates of more than 60 cu in/s (1 l/s) through the dynamic valves. Wind tunnel testing was conducted at speeds up through 13.1 ft/s (4 m/s) showing more than doubling of C_{lmax}. At low angles of attack and high flux rates, the airfoil produced net thrust for less than 4.1W of electrical power consumption.

Keywords: Piezoelectric Synthetic Jet Stall Suppression Drag Reduction Boundary Layer Control

NOMENCLATURE

Symbol	Description	Units
A, B, D	in-plane, coupled, bending laminate stiffnesses	lb/in, lb, in-lb (N/m, N, N-m)
b	span	in (cm)
c	chord	in (cm)
C_d	airfoil section drag coefficient	-
C_l	airfoil section lift coefficient	-
C_m	airfoil section pitching moment coefficient	-
C_μ	blowing momentum coefficient = $C_\mu = \dot{m}v_j / qs = 2\dot{V}v_j / cbv_\infty^2$	-
E	stiffness	GPa (msi)
l	length of side of square plenum actuator element	in (cm)
M	applied moment matrix	N-m/m (in-lb/in)
N	applied force matrix	N/m (lb/in)
Rn	Reynolds number	-
v	flow speed	ft/s (m/s)
V	volume of air pumped	ft^3 (m^3)
z	through thickness dimension	in (mm)
α	angle of attack	deg
ε	laminate in-plain strain	µstrain
κ	laminate curvature	rad/in (rad/m)
Λ	piezoelectric free element strain	µstrain
σ	stress	msi (GPa)

Subscripts

a	actuator
j	jet
l	laminate
s	steady
u	unsteady
∞	freestream

Smart Structures and Materials 2005: Smart Structures and Integrated Systems,
edited by Alison B. Flatau, Proc. of SPIE Vol. 5764 (SPIE, Bellingham, WA, 2005)
0277-786X/05/$15 · doi: 10.1117/12.599094

Downloaded from SPIE Digital Library on 21 May 2010 to 131.180.130.114. Terms of Use: http://spiedl.org/terms

1. INTRODUCTION

Boundary layer control (BLC) has been the subject of study, experimentation and regular publication for more than 75 years.[1-8] Early experiments on aerodynamic bodies sporting slots, holes or other perforations have been conducted regularly to improve aerodynamic characteristics. The overall goals of the various forms of BLC have typically been centered on methods designed to reduce overall drag and/or delay or eliminate flow separation or stall on wings and other aerodynamic shapes. Fig. 1 shows a generic airfoil operating with both separated flow and with attached flow via BLC. Many different configurations of suction and blowing mechanisms have been considered over the past 75 years. These methods have been shown to increase maximum lift coefficients to more than $C_l > 4$. References 1 – 8 also show that at higher flow coefficients, drag could be completely nulled, resulting in essentially dragless wing sections.

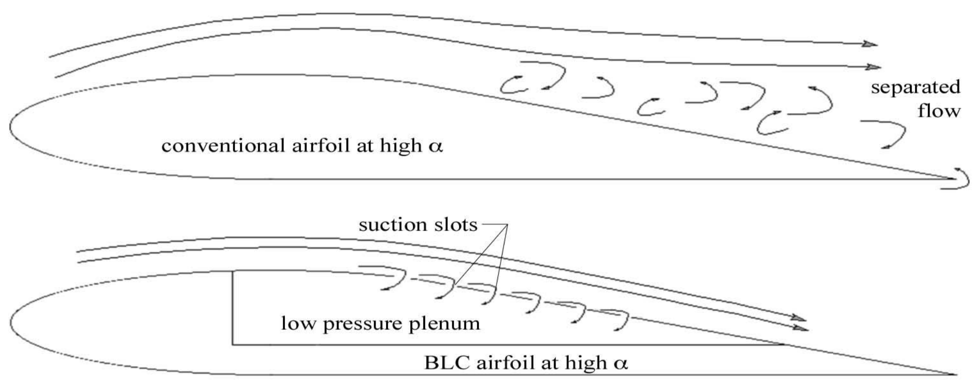

Fig. 1 Conventional and Generic BLC Airfoil Sections at High Angles of Attack

This general form of aerodynamic enhancement was put to the test in the early ‘60’s. The Northrop X-21A was specifically commissioned to showcase the tremendous benefits which can be obtained from BLC techniques. Two WB-66Ds were extensively modified by the Northrop Corporation as test vehicles for laminar flow control systems. The aircraft were fitted with a completely new wing of increased span and area, with a sweep reduced from 35 degrees to 30 degrees as shown in Fig. 2. The wings had a series of span-wise slots through which turbulent boundary-layer was sucked away, resulting in a smoother laminar flow operation, hopefully resulting in reduced drag, better fuel economy, and longer range. The underwing podded J71 engines were removed and replaced by a pair of 9490 lb.s.t (42kN) General Electric XJ79-GE-13 turbojets mounted in pods attached to the rear of the fuselage sides. Bleed air from the J79 engines was fed into a pair of underwing fairings, each of which housed a bleed-burn turbine which sucked the boundary layer air out through the wing slots. Testing proved that the overall concept was feasible, and a substantially improved range was obtained. However, it was found essential to keep the tiny wing slots spotlessly clean for effective operation, and this and other maintenance difficulties made the concept too costly for practical applications.

Fig. 2 The Northrop X-21A Boundary Layer Control Demonstrator Aircraft[9,10]

Although atmospheric fouling and maintenance problems severely degraded performance and rendered the BLC system of the X21A impractical, new attempts at BLC have been made by using Synthetic Jets (SJ). These devices employ no source or sink effect via a net flux of air continuously through the airfoil. Rather, the SJ

Downloaded from SPIE Digital Library on 21 May 2010 to 131.180.130.114. Terms of Use: http://spiedl.org/terms

approach extracts airflow from a local airstream, ingests it into a form of plenum or mainfold, then via the action of a pumping mechanism, generally expels the air through the orifice through which it was ingested. More than a decade of consistent research on various forms of SJ actuators has yielded some promising results from C_{lmax} enhancement through flow reattachment and drag reduction.[11-22] Figure 3 shows a generic schematic of a typical synthetic jet system.

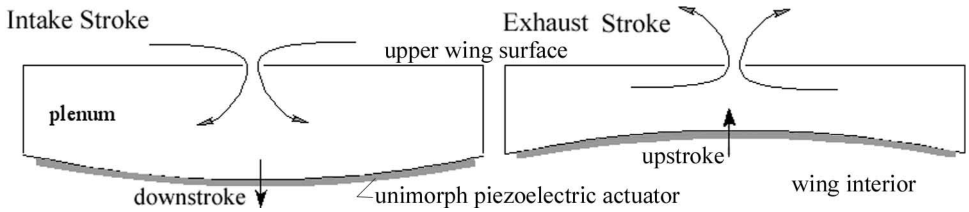

Fig. 3 General Arrangement of a Generic Normal Synthetic Jet (NSJ) Actuator

Fig. 3 shows a Normal Synthetic Jet (NSJ) plenum driven by a piezoelectric pumping mechanism composed of a single unimorph piezoelectric diaphragm. The piezoelectric diaphragm is designed so that as an electric field is applied to the piezoelectric element, the sheet will expand (left figure). As the polarity is reversed, the piezoelectric element contracts, driving the diaphragm upwards, thereby expelling air through the orifice. Although the concept has been shown to increase lift coefficients by more than 30% along with similar drag reductions, once again, the NSJ concept is susceptible to atmospheric fouling with bugs, dirt, dust, debris and ice as was the X-21A. In addition to operational woes, the effectiveness of NSJ actuators has been shown to be a strong function of local flow conditions including local turbulence levels, Reynolds numbers, Mach numbers and often flow history. These high sensitivities induce severe problems in terms of maintenance of high C_{lmax} or low C_{do} over differing flight conditions. Accordingly, although NSJ's and older forms of BLC have been shown to have some degree of success, a new approach is needed to bring the benefits of lift enhancement and drag reduction through BLC without any of the detracting characteristics.

2. PLENUM DESIGN AND STATIC MODELING

2.1 Tangential Synthetic Jet Design

To skirt the problems of atmospheric fouling, a series of tests were conducted on SJ's which employed dynamic members on the surface of the airfoil via moving stainless steel valve assemblies of 1mil (25µm) thickness and nominal slot height, vibrating vertically up to 5 mils (127µm) off the surface.[23] These tests showed that when exposed to dust particles from 1 to 10µm in diameter, after more than 80 hrs of testing, no particles either clogged or accumulated within the area of the valves on either the upstream or downstream sides of the valves. This was due primarily to the dynamic motions of the valves which were constantly in motion during operation. These motions effectively "swept away" any particles which might accumulate near the entrance or exit slots.

Another challenge of the NSJ actuators comes from the property of blowing normal to the aerodynamic surface. This normal blowing occasionally induces counterrotating streamwise vortices. However, just as often, such normal blowingblows off and otherwise separates the flow. To counter this tendency, a valve assembly was designed so that airflow is ingested on the upwind side and expelled on the downwind side of the valve mechanism. Figure 4 shows the overall schematic of the Dynamic Tangential Synthetic Jet (DTSJ) design. As can be seen from Fig. 4, the mechanism employs unique, dynamic fluid-structure interactions so as to effectively pump flow in the flow direction. The DTSJ system cycle begins with a downstroke of the piezoelectric diaphragm. This downstroke induces a reduced pressure distribution on the valve which partially bows the downstream side of the valve in towards the plenum. The downward deflection of the downstream side of the valve causes the upstream and support sections of the valve to rotate so that the upwind portion of the valve opens up to ingest oncoming flow. As the diaphragm reaches the bottom of the stroke, the static pressure difference over the valve is eliminated, causing the valve to lie tangential to the flow. Then as the diaphragm begins an upstroke, the pressure in the plenum is increased which causes the downwind side of the valve to be pushed open and expel air in a downstream direction. As the valve rotates, the upwind side of the valve seals tight, therefore preventing an upwind expulsion of air. After the diaphragm reaches its limit, once again, the valve will lay tangential to the flow, just prior to the start of another cycle.

Downloaded from SPIE Digital Library on 21 May 2010 to 131.180.130.114. Terms of Use: http://spiedl.org/terms

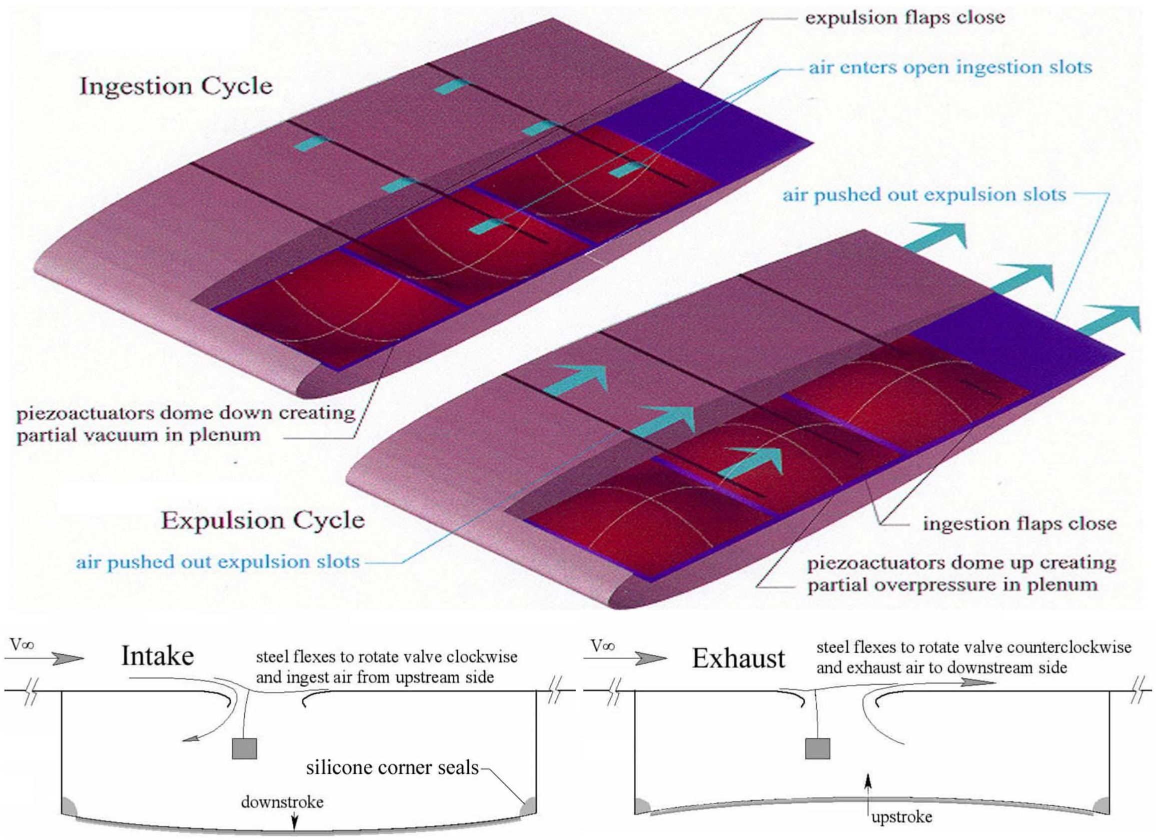

Fig. 4 Dynamic Tangential Synthetic Jet (DTSJ) Actuation Concept

As can be seen in Fig. 4, silicone corner seals are used to maintain structural connectivity between the diaphragms and the fiberglass sidewalls with minimal contribution to overall structural stiffness. The operational characteristics and principles of this and related DTSJ devices are described further in Ref. 24.

2.2 Static Diaphragm Modeling and Volume per Stroke Estimation

The static behavior of the piezoelectric diaphragm is easily captured by using classical laminated plate theory (CLPT) models. The diaphragm is made from two primary components: a piezoelectric actuator sheet bonded to a stainless steel foil substrate. As the piezoelectric sheet is commanded to expand or contract, the diaphragm deflects up and down, thereby pumping air through the stainless steel valve. The gross behavior of the device can be captured easily by the techniques described in Ref. 25 and 26. Assuming an unloaded structure and using CLPT methods, the following holds. The applied forces and moments may be balanced by stress distributions which are distributed through the thickness of the element

$$N = \int \sigma dz \qquad M = \int \sigma z dz \tag{1}$$

Actuator in-plane forces and moments (a) can be expressed as a balance with external forces and moments (ex) and forces and moments due to mismatches in coefficients of thermal expansion (t). These factors will generate in-plane laminate strains, ε and curvatures, κ.

$$\begin{Bmatrix} N \\ M \end{Bmatrix}_{ex} + \begin{Bmatrix} N \\ M \end{Bmatrix}_{a} + \begin{Bmatrix} N \\ M \end{Bmatrix}_{t} = \begin{bmatrix} A & B \\ B & D \end{bmatrix}_{l} \begin{Bmatrix} \varepsilon \\ \kappa \end{Bmatrix}_{l} \tag{2}$$

If the external forces and moments are ignored along with thermal variations, equation 2 can be reduced to:

$$\begin{bmatrix} A & B \\ B & D \end{bmatrix}_{l} \begin{Bmatrix} \varepsilon \\ \kappa \end{Bmatrix} = \begin{bmatrix} A & B \\ B & D \end{bmatrix}_{a} \begin{Bmatrix} \Lambda \\ 0 \end{Bmatrix} \tag{3}$$

Downloaded from SPIE Digital Library on 21 May 2010 to 131.180.130.114. Terms of Use: http://spiedl.org/terms

Expansion of equation 3 considering conventionally attached isotropic piezoelectric (CAP) actuators shows that shear and twist terms go to zero. Because free expansion piezoelectric strains, Λ, are typically equal for most types of CAP elements, equation 4 can be reduced to equation 5.

$$\begin{bmatrix} A_{11} & A_{12} & 0 & B_{11} & B_{12} & 0 \\ A_{12} & A_{11} & 0 & B_{12} & B_{11} & 0 \\ 0 & 0 & A_{66} & 0 & 0 & B_{66} \\ B_{11} & B_{12} & 0 & D_{11} & D_{12} & 0 \\ B_{12} & B_{11} & 0 & D_{12} & D_{11} & 0 \\ 0 & 0 & B_{66} & 0 & 0 & D_{66} \end{bmatrix}_l \begin{Bmatrix} \varepsilon_{11} \\ \varepsilon_{22} \\ \varepsilon_{12} \\ \kappa_{11} \\ \kappa_{22} \\ \kappa_{12} \end{Bmatrix} = \begin{bmatrix} A_{11} & A_{12} & 0 & B_{11} & B_{12} & 0 \\ A_{12} & A_{11} & 0 & B_{12} & B_{11} & 0 \\ 0 & 0 & A_{66} & 0 & 0 & B_{66} \\ B_{11} & B_{12} & 0 & D_{11} & D_{12} & 0 \\ B_{12} & B_{11} & 0 & D_{12} & D_{11} & 0 \\ 0 & 0 & B_{66} & 0 & 0 & D_{66} \end{bmatrix}_l \begin{Bmatrix} \Lambda_{11} \\ \Lambda_{22} \\ 0 \\ 0 \\ 0 \\ 0 \end{Bmatrix} \tag{4}$$

$$\begin{bmatrix} A_{11}+A_{12} & B_{11}+B_{12} \\ B_{11}+B_{12} & D_{11}+D_{12} \end{bmatrix}_l \begin{Bmatrix} \varepsilon \\ \kappa \end{Bmatrix} = \Lambda \begin{bmatrix} A_{11}+A_{12} \\ B_{11}+B_{12} \end{bmatrix}_a \tag{5}$$

If the total curvature of the plenum element is assumed to be relatively small, then a simple closed-form expression for volume drawn into the plenum from top dead center of the stroke to bottom dead center follows, assuming a parabolic form factor:

$$V = \frac{8l^3}{9} \tan\left[\frac{\Lambda\left(l/4 \right)}{A_l D_l - B_l^2} \left(A_l B_a - B_l A_a \right) \right] \tag{6}$$

3. WING SECTION DESIGN AND FABRICATION

3.1 Overall Design

The design of the DTSJ actuator system within a generic wing section was accomplished in several stages. The first was to lay out the overall arrangement of the plenums within a benchmark 1 ft (30.5cm) chord, 6" (15cm) semispan NACA 0012 wing section. Because accurate aerodynamic modeling of unsteady, viscous, separated flows interacting with active and aeroelastic structures was beyond the funding levels available for this study, a versatile experimental model was conceived and fabricated. Given that the 1 mil (25µm) thick valve assemblies shown in Fig. 4 lie well within local boundary layers over the wing section, overall flow will not be disturbed by a plethora of valves, especially if a standard roughening strip is used to simulate higher Reynolds number flow as described in Ref. 27. Because the NACA 0012 experiences a mixture of several stall mechanisms, valve assemblies were placed along the chord to suppress several of those mechanisms simultaneously. Fig. 5 shows valves placed from 15%c to the trailing edge of the wing section.

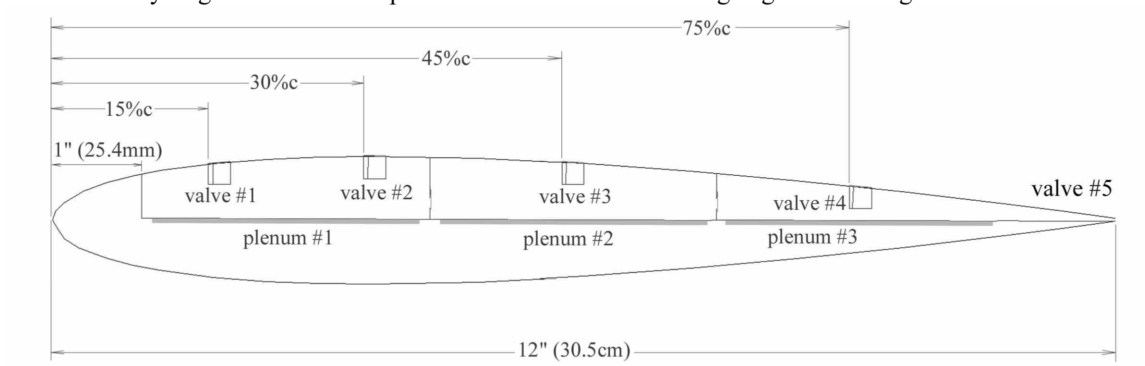

Fig. 5 General Arrangement of DTSJ System in the NACA 0012 Wing Section

The reader is asked to note that any of the valves could be closed at any time via the application of 0.5mil (12µm) thick tape thereby sealing the orifice. There are also two cutouts which allows the three plenums to freely transfer air between them. A close-up of the plenum geometry shows that 2.85" (7.24cm) square CAP

Downloaded from SPIE Digital Library on 21 May 2010 to 131.180.130.114. Terms of Use: http://spiedl.org/terms

actuator elements were bonded to 3.25” (8.26cm) square plenums. The 0.25” (6.4mm) chord stainless steel valve was designed across a 0.20” (5.3mm) orifice. The stainless steel valve was bonded to a structurally stiff support as shown in Fig. 6.

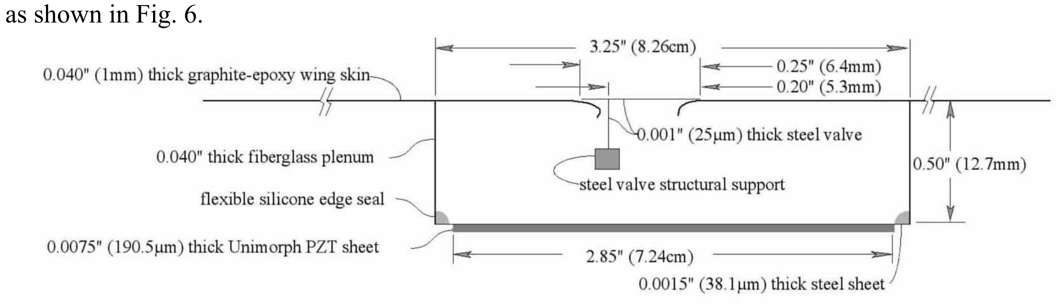

Fig. 6 Plenum Structural Details

3.2 Test Article Fabrication

The core of the test article is the valve assembly which was fabricated from a pair of stainless steel sheets as shown in Fig. 7.

Fig. 7 Stainless Steel Valve Assembly

The wing section was fabricated from Cyanimide 123 graphite-epoxy composite structures and finished to a 1 mil (25μm) surface tolerance. The three plenums were attached to the inside of the graphite-epoxy skins with Hysol 123 epoxy resin as shown in Fig. 8.

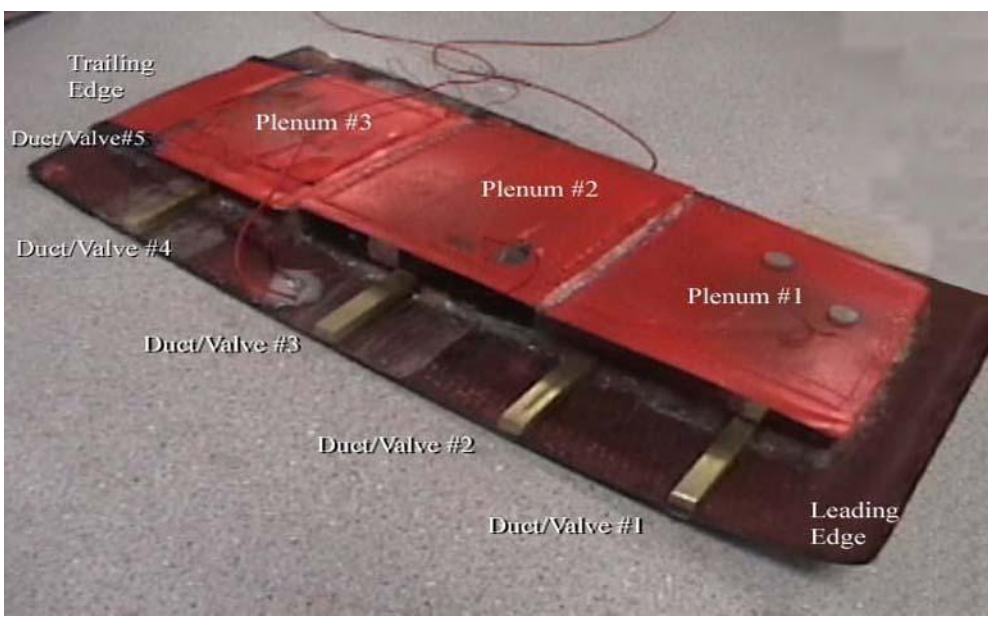

Fig. 8 Underside of the DTSJ Test Article

Downloaded from SPIE Digital Library on 21 May 2010 to 131.180.130.114. Terms of Use: http://spiedl.org/terms

Four brass ducts are seen extending laterally from the plenums to carry air pumped by the plenums to and from the wing skin. The trailing edge valve assembly is seen as a continuous sheet spanning the airfoil. The valves are sealed at the ends where the brass ducts come to a close as shown in Fig. 9.

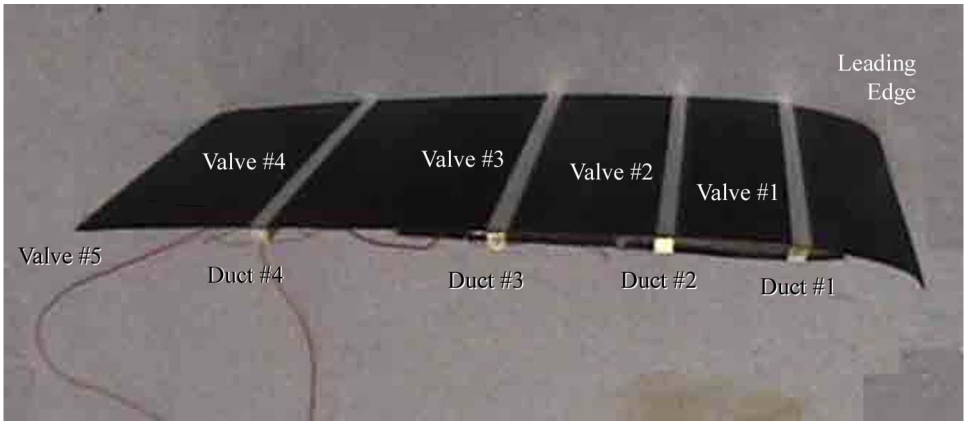

Fig. 9 Upper Surface of the DTSJ Test Article

4. EXPERIMENTAL TESTING

4.1 Test Set-Up

The NACA 0012 test article was suspended between two walls of a 1ft (30cm) low speed, low Reynolds number wind tunnel at speeds up to 13.1 ft/s (4m/s). Lift was measured via a force balance system with an accuracy of 2.2E-6 lbf (±1mgmf). Drag was determined by a wake-rake system with 1.5E-6 psi (0.01Pa) sensitivity in a momentum deficit integration. A boundary layer splitter plate reduced local boundary layers on side walls to under 0.02% span.

Power was supplied to the plenums via a signal generator driving a Piezo Systems EPA-104 high voltage amplifier. A sine signal of varying frequency was supplied to the piezoelectric actuators from 10V to 240V peak-to-peak.

4.2 Test Procedures

Quasi-static testing was conducted on the piezoelectric plenums at a frequency of 1 Hz. Quarter-wavelength laser mirrors were placed at the edges of the piezoelectric elements so that deflections could be measured to ±0.01°. Plenum deflections were measured with non-contact proximity detectors to 2mil (50µm) accuracy. Static pumping volumes were measured fluidically in a propanol bath.

Dynamic testing was conducted in ambient air conditions at 72°F (22°C) by using laser Doppler velocimetry integrated across the inlets and exits of the plenums. Although measurements were made at rates in excess of 1,000 samples/sec. over the 6” (15cm) span, they were taken in 9 separate scans across the leading and trailing edges of valves #1 – 4 and at the exit of valve #5.

5. TEST RESULTS

5.1 Quasi-Static Bench Test Results

Quasi-static bench testing was conducted with a 1 Hz sine signal applied to the plenums to generate periodic deflections. Deflection measurements were made using laser-reflection techniques while volumetric measurements were made using fluidic measurement techniques described above. Fig. 10 shows good correlation between theory and experiment between measured and predicted deflection levels. It is thought that the decrement in the measured deflections with respect to the predicted deflections is induced by the finite stiffness of the silicone seals at the edges. Fig. 10 also shows more than 5cc of volume pumped per half stroke at field strengths in excess of 500 V/mm.

Downloaded from SPIE Digital Library on 21 May 2010 to 131.180.130.114. Terms of Use: http://spiedl.org/terms

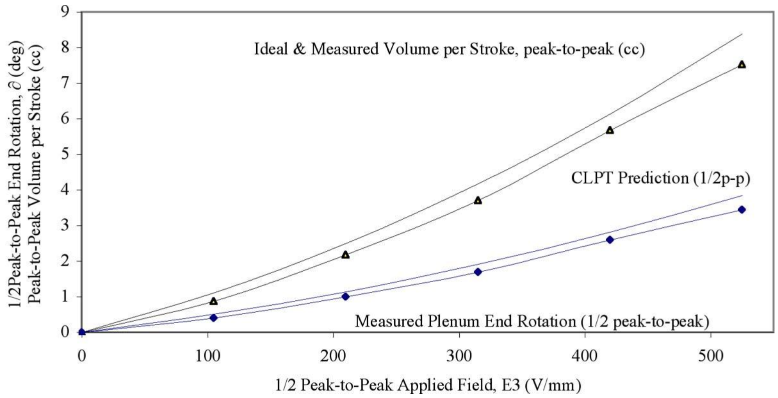

Fig. 10 Predicted and Measured Quasi-Static Diaphragm End Rotation and Volume per Stroke

5.2 Dynamic Bench Test Results

Dymamic bench testing was conducted using laser reflection techniques and laser Doppler velocimetry. Figure 11 shows the dynamic test results of a single plenum driving a single valve assembly. Dynamic testing was conducted at ±40V peak-to-peak at frequencies ranging from 1 to 350 Hz.

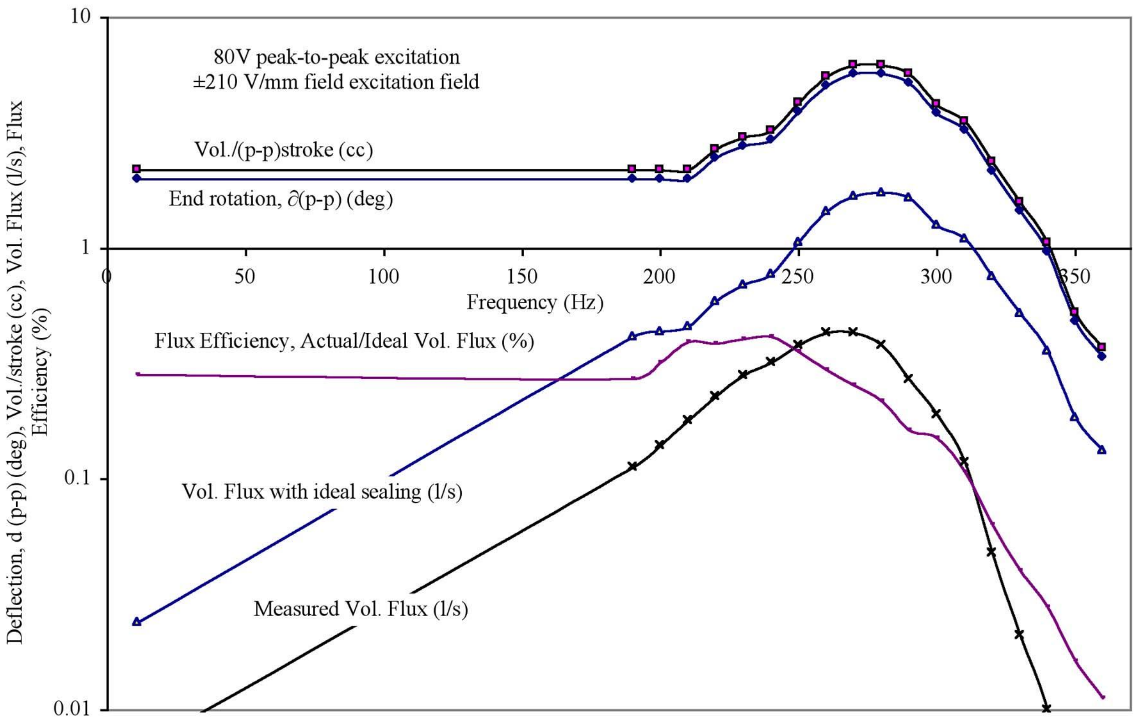

Figure 11 Dynamic Bench Test Results

Fig. 11 shows relatively steady volume pumped per cycle of approximately 2cc/stroke below 200 Hz, which is well below the resonance peak at approximately 270 Hz. Aerodynamic damping and fluid pumping is assumed to knock the spike from the resonance peak at this range, resulting in maximum volume flux rates of 430cc/s. Although a considerable amount of air was ejected through razor thin slots, the overall pumping efficiency was relatively low, ranging from 28% at low frequencies, peaking at 41.3% at 240 Hz. From detailed flow observations, it is obvious that incomplete valve sealing is the mechanism which induces the greatest amount of losses. At the maximum pumping rate of 430 cc/s, ejector valve slot heights were observed at 10.2mil (260μm), resulting peak flow speeds of 75.5 ft/s (23m/s). Because of ejector valve closing, nominal flow speeds through the valve assemblies were approximately 56.1 ft/s (17.1m/s).

Downloaded from SPIE Digital Library on 21 May 2010 to 131.180.130.114. Terms of Use: http://spiedl.org/terms

5.3 Wind Tunnel Test Results

Wind tunnel testing was conducted in a low turbulence, low speed wind tunnel up through speeds of 9.8 ft/s (3m/s). The nominal steady-state blowing coefficient achieved at 9.8 ft/s (3m/s) was $C_{\mu s} = 0.036$. Peak unsteady blowing coefficients were measured at $C_{\mu u} = 0.049$. Figure 12 shows the airfoil section at 16° angle of attack with the system off and the system on operating at 270 Hz, ±40V peak-to-peak. A titanium tetrachloride wipe was used on the leading edge of the airfoil to visualize the flow seen in Fig. 12.

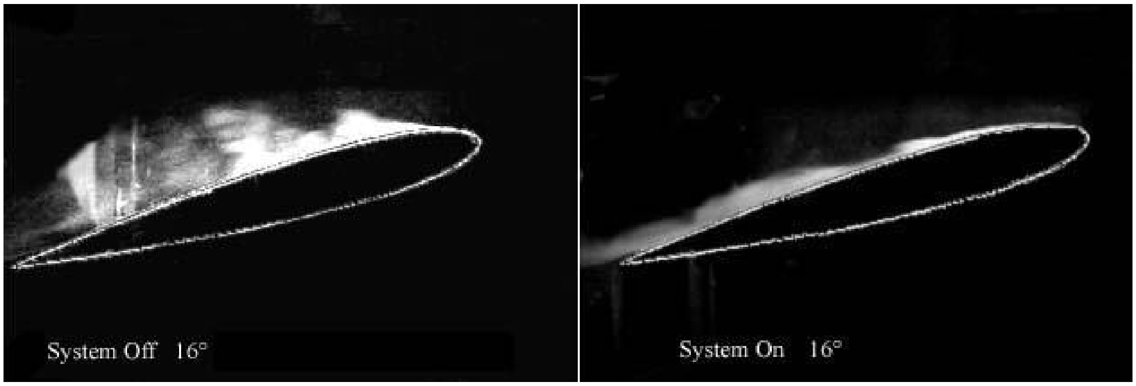

Figure 12 DTSJ System On and Off at 270 Hz, ±40Vp-p, 9.8 ft/s (3 m/s), Rn = 62,400

From Fig. 12, it is clear that at 16° angle of attack without the DTSJ system working, the flow encounters gross separation at the leading edge and does not reattach. With the system on, the flow is much more organized as it progresses downstream and stays attached, thereby inducing an enhancement of lift coefficient. Because five different valves could be turned on or off independently via the addition or removal of 0.5mil (12µm) thick sealing tape, there are 32 permutations of possibility for testing. Table 1 shows the test condition numbers corresponding to each of these conditions.

Table 1 Matrix of Test Conditions for Wind Tunnel Testing

Test Condition	1	2	3	4	5	6	7	8	9	10	11	12	13	14	15	16	17	18	19	20	21	22	23	24	25	26	27	28	29	30	31	32
Slot																																
1																	on	on	on	on	on	on	on	on	on	on	on	on	on	on	on	on
2									on	on	on	on	on	on	on	on									on	on	on	on	on	on	on	on
3					on	on	on	on					on	on	on	on					on	on	on	on					on	on	on	on
4			on	on			on	on			on	on			on	on			on	on			on	on			on	on			on	on
5		on		on		on		on		on		on		on		on		on		on		on		on		on		on		on		on

Data was sampled at a rate of 100 Hz with 1,000 samples being averaged for each data point. Wind tunnel test results showed significant peaks in lift coefficient with certain combinations of jet actuators on and off. From Fig. 13, it can be seen that the most effective dynamic synthetic jets are numbers 1, 2 and 5. It is thought that these combinations suppress the various types of stall mechanisms including a leading edge stall mechanism suppressed by DTSJ's 1 & 2 while the aft device suppresses trailing-edge stall. The reader is asked to note that the greatest levels of lift enhancement are seen with conditions, 10, 26, 30 and 32. In each of these conditions, DTSJ's 2 and 5 are active while some or none of the others are active. Fig. 13 also shows that C_{lmax} was increased from 1.13 with the system off to 2.04 with the system running – an 80% increase. Conversely, the action or inaction of valves #3 and #4 have barely noticeable effects throughout the operating range. Only when used in combination with the other mechanisms does their participation or lack thereof become important in influencing C_{lmax}. Because the mechanism which induces such significant jumps in lift coefficient is flow attachment, of course, the drag coefficient is similarly aided.

Figure 14 shows the effect of the various combinations of DTSJ's on drag reduction. As one of the three most effective configurations with a more gentle stall mechanism, configuration 26 was chosen for this portion of the study. A sweep of applied power shows steady trends demonstrating that the DTSJ concept does not rely

Downloaded from SPIE Digital Library on 21 May 2010 to 131.180.130.114. Terms of Use: http://spiedl.org/terms

upon point singularities in the flow field, but can be used over a wide range of angles of attack and power settings to improve flow attachment, thereby enhancing lift and decreasing drag. The reader will note that at 100V peak-to-peak actuation, the drag coefficients actually become negative, indicating that the airfoil was actually generating thrust.

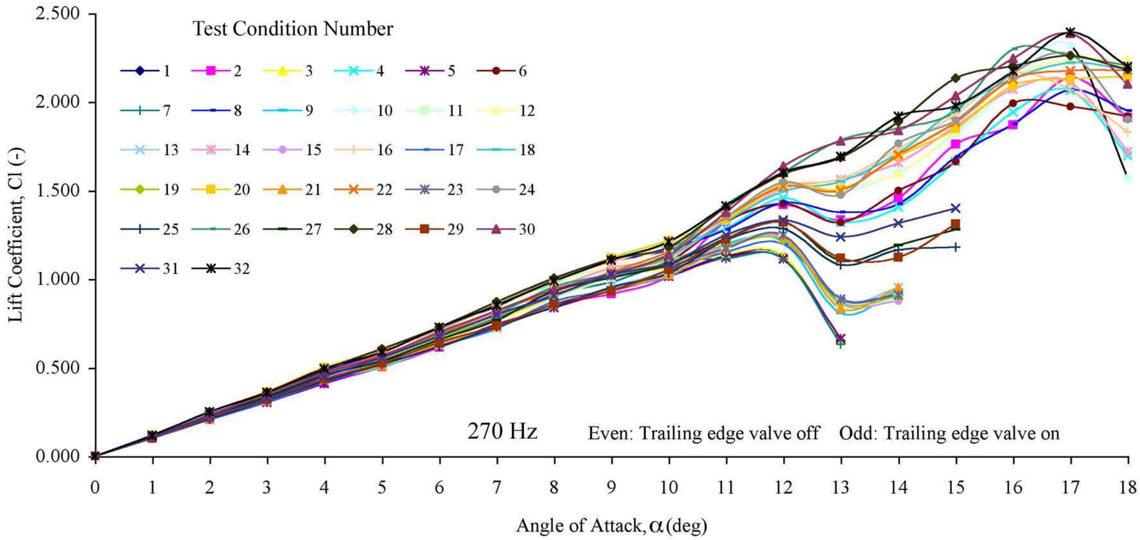

Figure 13 Dynamic Lift Enhancement at 270 Hz, 9.8 ft/s (3m/s), Configurations 1 through 32

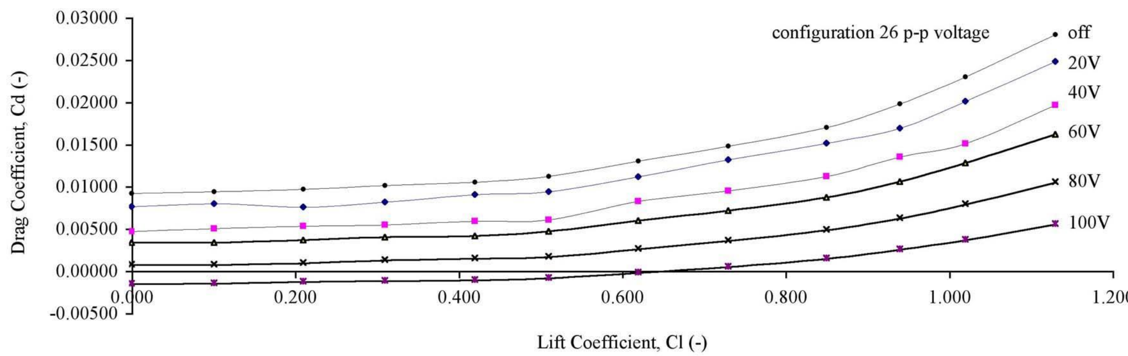

Figure 14 Drag Reduction at 270 Hz, 9.8 ft/s (3m/s), Rn = 62,400 Configuration 26 with Excitation Voltage

A sweep of airspeed shows that, although the drag polar is shifted a few percent up and down with increasing or decreasing airspeed, there are no fundamental flow instabilities or hard breaks in trends even with a quadrupling of the Reynolds number.

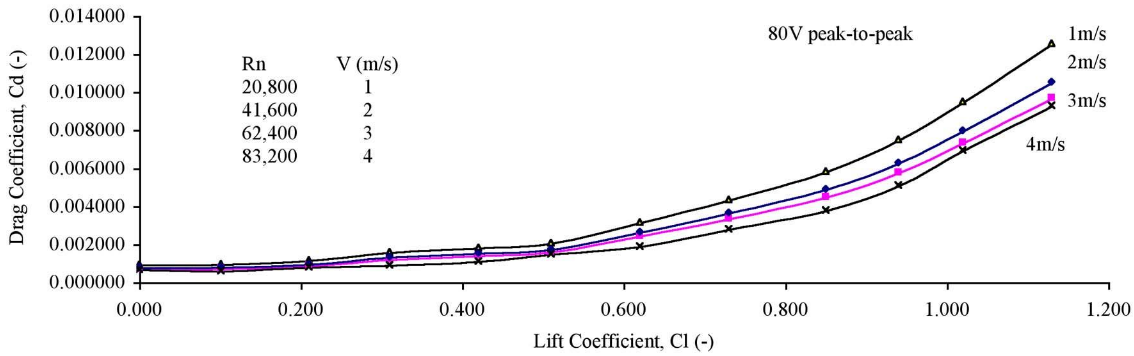

Figure 15 Drag Polar at 270 Hz, 3.2 ft/s (1m/s) through 13 ft/s (4m/s) Configuration 26 at 80 V Peak-to-Peak

Downloaded from SPIE Digital Library on 21 May 2010 to 131.180.130.114. Terms of Use: http://spiedl.org/terms

It can be seen that although the benefits are substantial, the 4.1W of electrical power consumed to produce the data of Figures 13, 15 is modest. In addition to power consumption, one of the more important characteristics of the gross performance of the airfoil relates to lift-to-drag ratio. Because configuration 26 at 100 V peak-to-peak excitation, 3m/s flow speed, the airfoil produces thrust at low angles of attack, that trendline was omitted (which would yield an infinite lift-to-drag ratio). Rather, data is shown up to 80V peak-to-peak excitation below:

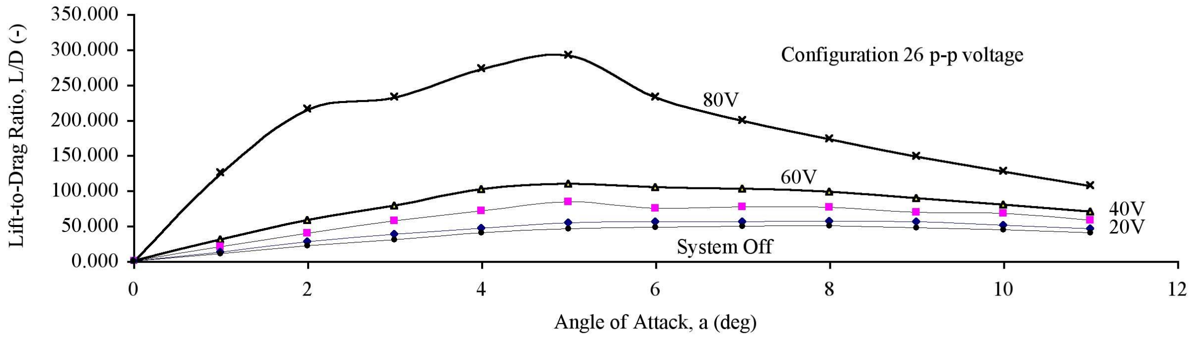

Figure 16 Enhancement of Lift-to-Drag Ratio, 270 Hz, 9.8 ft/s (3m/s) Configuration 26 with Excitation Voltage

CONCLUSIONS

It can be concluded that the Dynamic Tangential Synthetic Jet (DTSJ) system works very well over a wide range of angles of attack and flow conditions, ingesting airflow from the upstream direction and dynamically expelling it in the downstream direction, tangential to the airfoil surface through razor-thin stainless steel valves. The system was proven on a 12" (30.5cm) chord, 6" (15cm) span NACA 0012 airfoil section with three 3.25" (8.23 cm) square plenums driving five 1 mil (25µm) thick DTSJ valve assemblies. Static testing showed that the system was capable of generating pumping volumes in excess of 7cc per plenum actuation cycle quasi-statically with good correlation between Classical Laminated Plate Theory (CLPT) estimations and theory. With a resonance peak near 270 Hz, the pumping rate surpassed 430cc/s per plenum, resulting in tangential valve flow velocities in excess of 75 ft/s (23m/s) per open valve assembly. A sweep of the 32 different combinations of valve conditions showed that active valves near the 15% and 30% chord and the trailing edge were most effective while those at 45% and 75%c were fundamentally ineffective. Wind tunnel testing showed that at 80V peak-to-peak excitation levels, 270 Hz, 9.8 ft/s (3m/s) using the most effective valve configuration, C_{lmax} was increased by more than 80% while α_{stall} was raised by 42%. A drag study showed that at 100V peak-to-peak excitation levels, net airfoil thrust was generated. Tests at 270 Hz, 80V peak-to-peak excitation in flow speeds from 3.2 ft/s (1 m/s) through 13 ft/s (4m/s), showed that although C_{lmax} decreased with increasing speed by more than 20% because of reduced blowing coefficients, C_{do} was essentially unchanged throughout the entire range. For flow conditions with positive C_d, it was shown that L/D's in excess of 300 could be achieved for only 4.1W of electrical power consumption.

ACKNOWLEDGMENTS

The authors would like to acknowledge the outstanding contributions of the many students and colleagues who helped with this study including Mr. Christoph Burger, Ross McMurtry, Roelof Vos, Koen Artois, Dr. R. Steven Gross and Mr. Bill Holbrook. This study was sponsored by the AAL and the Technical University of Delft, Netherlands.

REFERENCES

1. Knight, Montgomery and Bamber, Millard J., "Wind Tunnel Tests on Airfoil Boundary Layer Control Using a Backward Opening Slot," NACA TN No. 323, 1929.
2. Schrenk, Oskar, "Experiments with a Wing Model from Which the Boundary Layer Is Removed by Suction, NACA TM No. 534, 1929.
3. Schrenk, Oskar, "Experiments with a Wing from Which the Boundary Layer Is Removed by Suction, NACA 634, 1931.

Downloaded from SPIE Digital Library on 21 May 2010 to 131.180.130.114. Terms of Use: http://spiedl.org/terms

4. Schrenk, Oskar, "Experiments with Suction-type Wings, NACA TM No. 773, 1929.
5. Bamber, Millard J., "Wind-tunnel Tests on Airfoil Boundary Layer Control Using a Backward-opening Slot," NACA Report No. 385, 1931.
6. Quinn, John H., Jr. "Tests of the NACA 65_3-018 Airfoil Section with Boundary-Layer Control by Suction," NACA CB No. L4H10, 1944 (Wartime Report No. L-209).
7. Quinn, John H., Jr., "Wind-tunnel Investigation of Boundary-layer Control by Suction on the NACA 65_3-418, a = 1.0, Airfoil Section with a 0.29 Airfoil-chord Double Slotted Flap, NACA TN No. 1071, 1946.
8. Quinn, John H., Jr., "Tests of the NACA 64_1A212 Airfoil Section with a Slat, a Double Slotted Flap, and Boundary-layer Control by Suction, NACA TN No. 1293, 1947.
9. Miller, J., "The X-Planes, X-1 to X-45," Midland Publishing, London, England, 2004.
10. Braslow, Albert, "A history of suction-type laminar-flow control with emphasis on flight research," published by NASA History Division, Office of Policy and Plans, NASA Headquarters, Washington, DC 1999.
11. Amitay, M., Smith, D.R., Kibens, V., Parekh, D.E. and Glezer, A. "Modification of the Aerodynamics Characteristics of an Unconventional Airfoil Using Synthetic Jet Actuators", *AIAA Journal*, Vol. 39, No. 3, pp. 361-370, March 2001.
12. Amitay, M. and Glezer, A. "Role of Actuation Frequency in Controlled Flow Reattachment over a Stalled Airfoil", *AIAA Journal*, Vol. 40, No. 2, pp. 209-216, 2002.
13. Glezer, A. and Amitay, M. "Synthetic Jets", *Annual Review of Fluid Mechanics*, 2002.
14. Amitay, Michael, and Glezer, Ari, US Pat. 6,412,732 "Apparatus and method for enhancement of aerodynamic performance by using pulse excitation control of synthetic jet actuators," July 2, 2002.
15. Amitay, M., Smith, D., Kibens, V., Parekh, D. and Glezer, A., "Aerodynamic Flow Control of Bluff Bodies Using Synthetic Jet Actuators". Proceedings of the IUTAM Symposium on Mechanics of Passive and Active Control, held in Gottingen, Germany, September 7-11, 1998.
16. Amitay, M. and Glezer, A. " Aerodynamic Flow Control of a Thick Airfoil using the synthetic Jet Actuators", Proceedings of the 3rd ASME/JSME Joint Fluids Engineering Conference, San Francisco, California, July 18-23, 1999.
17. Smith, D. R., Amitay, M., Kibens, V., Parekh D.E. and Glezer, A. "Modification of Lifting Body Aerodynamics by Synthetic Jet Actuators", AIAA Paper 98-0209, 1998.
18. Amitay, M., Kibens, V., Parekh, D.E. and Glezer, A, "Flow Reattachment Dynamics over a Thick Airfoil Controlled by Synthetic Jet Actuators", AIAA Paper 99-1001, 1999.
19. Amitay, M., Pitt, D., Kibens, V., Parekh, D.E. and Glezer, A., "Control of Internal Flow Separation using Synthetic Jet Actuators", AIAA Paper 2000-0903, 2000.
20. Honohan, A. M., Amitay, M. and Glezer, A. "Aerodynamic Control using Synthetic Jets", AIAA Paper 2000-2401, 2000.
21. Chatlynne, E., Rumigny, N., Amitay, M. and Glezer, A., "Virtual Aero-Shaping of a Clark-Y Airfoil using Synthetic Jet Actuators", AIAA Paper 2001-0732, 2001.
22. Amitay, M., Horvath, M., Michaux, M. and Glezer, A., "Virtual Aerodynamic Shape Modification at Low Angles of Attack using Synthetic Jet Actuators", AIAA Paper 2001-2975, 2001.
23. Corpening, J. and Reasonover, C., "An Experimental and Analytical Investigation of Boundary Layer Reattachment using Piezoelectric Synthetic Jet Actuators," AIAA Region II Conference, Kitty Hawk, NC, April 2001.
24. Barrett, R., Corpening, J., and Reasonover, C., "Method and Apparatus for Boundary Layer Reattachment using Piezoelectric Synthetic Jet Actuators," U.S. Patent 6,796,533, issued 28 September 2004.
25. Jones, R. M., "Micromechanical Behavior of a Lamina," *Mechanics of Composite Materials*, Hemisphere Publishing Corporation, New York, 1975.
26. Crawley, E. F. and De Luis, Javier, "Use of Piezoelectric Actuators as Elements of Intelligent Structures," *AIAA Journal,* Vol. 25, No. 10, Oct. 1987, pp. 987-997.
27. Von Doenhoff, A. E., Abbott, I. H., "Theory of Wing Sections," published by Dover Publications, New York, NY 1959.

Downloaded from SPIE Digital Library on 21 May 2010 to 131.180.130.114. Terms of Use: http://spiedl.org/terms